




Transition to quantum turbulence in oscillatory thermal counterflow of ^4He Š. Midlik ^{*}, D. Schmoranzner , and L. Skrbek *Faculty of Mathematics and Physics, Charles University, Ke Karlovu 3, 121 16 Prague 2, Czech Republic*

(Received 23 January 2021; revised 12 April 2021; accepted 13 April 2021; published 27 April 2021)

We report an experimental study of oscillatory thermal counterflow of superfluid ^4He and its transition to quantum turbulence inspired by the work of Kotsubo and Swift [*Phys. Rev. Lett.* **62**, 2604 (1989)]. We use a pair of transversally oriented second-sound sensors to provide direct proof that upon exceeding a critical heat flux, quantized vorticity is generated in the antinodes of the longitudinal resonances of the oscillating counterflow. Building on modern understanding of oscillatory flows of superfluid ^4He [D. Schmoranzner *et al.*, *Phys. Rev. B* **99**, 054511 (2019)], we re-evaluate the original data together with ours and provide grounds for the previously unexplained temperature dependence of critical velocities. Our analysis incorporates a classical flow instability in the normal component described by the dimensionless Donnelly number, which is shown to trigger quantum turbulence at temperatures below ≈ 1.7 K. This contrasts with the original interpretation based on the dynamics of quantized vortices, and we show that for oscillatory counterflow, such an approach is valid only at temperatures above ≈ 1.8 K. Finally, we demonstrate that the instabilities occurring in oscillatory counterflow are governed by the same underlying physics as those in flow due to submerged oscillators and propose a unified description of high Stokes number coflow and counterflow experiments.

DOI: [10.1103/PhysRevB.103.134516](https://doi.org/10.1103/PhysRevB.103.134516)**I. INTRODUCTION**

Quantum turbulence [1,2] in superfluid ^4He (He II) in the temperature range from ≈ 1 K to T_λ , where He II displays the two-fluid behavior, is easy to generate experimentally but challenging to understand in its entirety. In the frame of the two-fluid model, He II consists of two components: the viscous normal component of density ρ_n carrying all the entropy content of He II and the inviscid superfluid component of density ρ_s , with the total density $\rho = \rho_n + \rho_s$. This makes superfluid ^4He a complex system: One can expect an interplay of turbulent normal component of very low kinematic viscosity ν_n , obeying in some cases classical laws, and of inviscid superfluid component, behaving under quantum restrictions, with all rotational flow in the form of quantized vortices possessing angstrom-sized cores [3]. These line singularities, usually arranged in a complicated tangle, carry a single quantum of circulation $\kappa \cong 10^{-7} \text{ m}^2\text{s}^{-1}$ each. Vortex lines mediate the interaction between the two components via a mutual friction force acting at all relevant length scales; moreover, any thermal gradient in He II generates thermal counterflow.

Various forms of quantum turbulence in He II can be generated using mechanical and thermal drives [4]. Classical-like mechanical forcing (e.g., by towing or oscillating a grid or any bluff body such as a wire or a quartz tuning fork) usually [4] results in a *coflow*, the closest analog to classical viscous flows, in which the normal fluid and superfluid components move, on average, with the same mean velocity in the same direction. By combining mechanical and thermal driving, the

two components of He II can also be made to flow, on average, relative to each other [5], a situation called *counterflow*. The special case of counterflow with no net mass flow in the laboratory frame of reference called *thermal counterflow* is probably the most frequently investigated quantum flow since the pioneering experiments of Vinen [6]. In another special case called *pure superflow*, only a net flow of the superfluid component occurs in the experimental frame of reference, while the normal component remains statistically steady [7–9].

Additionally, as first shown by Kotsubo and Swift [10,11] and later by Chagovets [12], quantum turbulence can be generated in He II by applying a high-amplitude second sound in the longitudinal direction of a closed channel acting as a second-sound resonator. Here we present a similar experiment, however, with the addition of direct measurement of vortex line density, L , in the center of the resonator. Based on our results and subsequent analysis, taking into account experiments described in Refs. [10–12], we point out the close similarity of the underlying physics between quantum turbulence generated in an oscillating flow due to a bluff body [13,14] or U-tube oscillations [15] and by second sound, which involves a high Stokes number oscillatory flow of the normal component of He II in the resonator [16].

II. EXPERIMENTAL SETUP AND METHODS

The experimental volume of He II is contained in the 1-cm-wide brass channel of square cross section 3.2-cm long, a second-sound resonator, closed from both ends with brass plugs. We generate two different second-sound signals which we refer to as (i) longitudinal second sound, driven thermally at high amplitude along the longer dimension of the resonator,

^{*}midliks@o365.cuni.cz

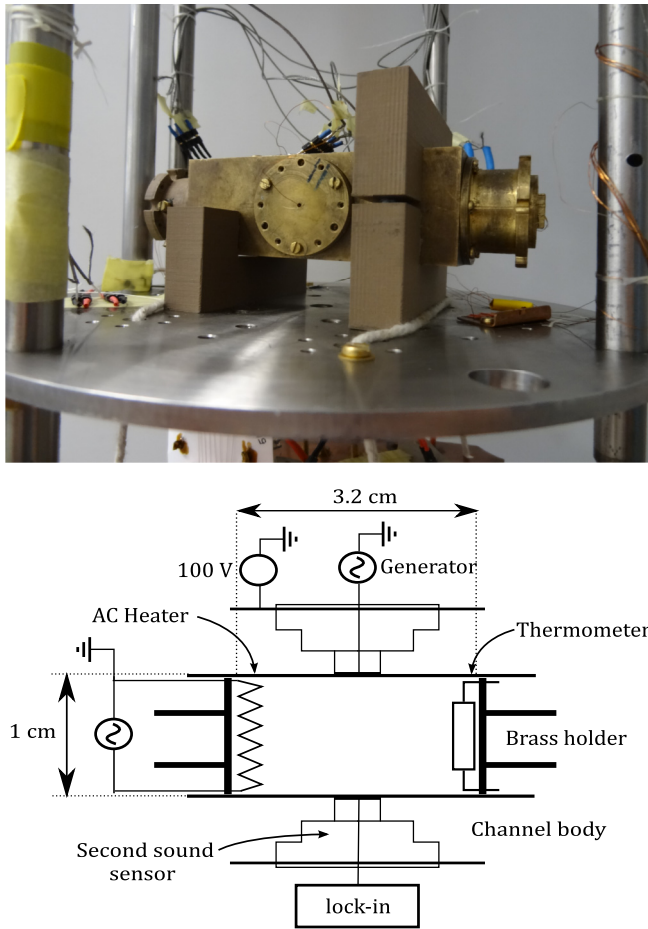


FIG. 1. Top: Photograph of the experimental brass cell with the transversal second-sound sensor holder on its front side and the heater and thermometer on the brass holders inserted from the left and right sides. Bottom: Schematic of the experimental cell arrangement. Longitudinal second-sound signal is generated by the resistive heater, forming a standing wave along the resonator, and probed by the sensitive resistance thermometer placed at the opposite end. Transversal second-sound signal is driven in the middle of the resonator perpendicularly to its length by one of two capacitive sensors acting as a generator with the opposing one used as a detector.

which is used for generation of quantized vorticity; and (ii) transversal (or detection) second sound, driven at low amplitude mechanically across the center of the resonator. A schematic view of the experiment is shown together with a photograph of the setup in Fig. 1.

The longitudinal second sound is driven by a flat heater of resistance $R \approx 50 \Omega$. It is made of a manganin wire and glued to one of the brass plugs at one end of the resonator. The applied ac voltage $U = U_0 \cos(\omega t)$ of angular frequency ω and amplitude U_0 results in radiation of a heat flux \dot{q} at 2ω . In a channel of constant cross section, A_s , the time-dependent heat flux is formally given as

$$\dot{q} = \dot{q}_{dc} + \dot{q}_{ac} \cos(2\omega t) = \frac{U_0^2}{2RA_s} [1 + \cos(2\omega t)], \quad (1)$$

resulting in radiation of (i) the ac temperature wave and (ii) the dc heat flux. The net dc heat flux is carried away from

the heater by the normal component of He II and causes steady thermal counterflow of some form, which we discuss in Sec. IV.

In a conventional counterflow channel of constant cross section, with one end open to the helium bath, from the conservation of energy, the counterflow velocity is found as

$$v_{CF} = \frac{\dot{q}_{dc}}{ST\rho_s}, \quad (2)$$

where \dot{q}_{dc} is the applied heat flux (power per unit area) and S and T denote, respectively, the specific entropy and the temperature of He II. The dc heat flux might generate quantized vorticity. This happens above the critical counterflow velocity v_0 ; the intensity of generated quantized vorticity is characterized by vortex line density, L , which follows the experimentally established [6] power law scaling,

$$L - L_0 = \gamma^2(T)(v_{CF} - v_0)^2, \quad (3)$$

where L_0 corresponds to the remnant vortex line density [17]. The dimensional coefficient $\gamma(T)$ (for the so-called T II state of thermal counterflow in relatively wide channels) has been experimentally established with about 20% accuracy [7].

The generated longitudinal second sound is detected by a semiconductor-based Ge/GaAs Microsensor TTR – G thermometer [18–20] biased with a constant current of $1 \mu\text{A}$, placed on the brass plug closing the opposite side of the resonator. The thermometer signal is measured using a Stanford SR830 lock-in amplifier at the expected frequency ω/π , i.e., at double frequency of the driving voltage. Under the assumption of linear damping of the second-sound wave, the maximum counterflow velocity reached in the antinodes of the second-sound wave is given by a similar equation as for steady counterflow, Eq. (2), enhanced by the quality factor Q of the second-sound resonator.

For the detection of quantum turbulence, we have built and further improved the traditional capacitive sensors; for details of their construction and readout method see Refs. [8,21] and references therein. In short, two identical sensors, serving as a transducer and receiver, are constructed from a $10\text{-}\mu\text{m}$ -thick nuclepore membrane, coated on one side with a 30- to 60-nm-thick layer of gold. It is stretched across a circular Delrin holder 1 cm in diameter and lightly pressed against a brass electrode. Its gold-plated side and the electrode constitute a parallel-plate capacitor of typically 30 to 100 pF. The two sensors face each other across the resonator in the middle of its length (see Fig. 1), one being driven by an ac voltage superimposed on a high dc bias of 100 V, while the voltage signal from the other sensor is read using a lock-in amplifier. Assuming a random vortex tangle, homogeneous across the width of the channel, the vortex line density in the probed volume is then obtained from the level of attenuation of the standing transversal second-sound wave as

$$L = \frac{6\pi \Delta f}{\kappa B} \left(\frac{A}{A_0} - 1 \right), \quad (4)$$

where Δf and A_0 are the full width (FWHM) and the amplitude of the second-sound signal measured without the application of the longitudinal drive, A is the amplitude of the attenuated signal, κ is the circulation quantum, and B is the tabulated [22] mutual friction coefficient. We note that Eq. (4)

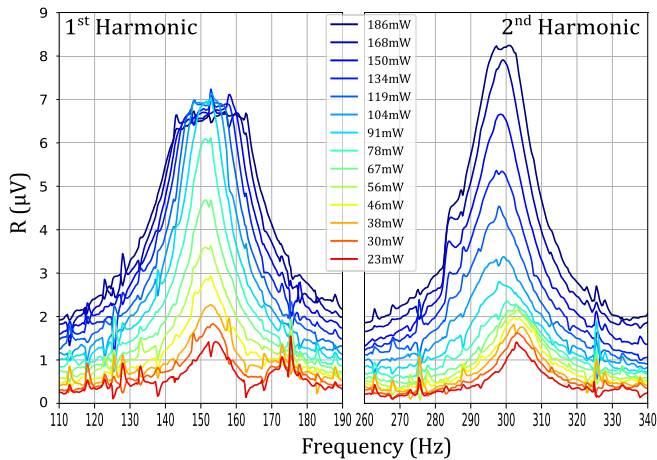


FIG. 2. The amplitudes of first two resonant modes of longitudinal second sound measured at 1.65 K and plotted against the frequency of the ac driving voltage supplied to the heater. The crossover between two different peak shapes is displayed: (i) Lorentzian shape in the linear damping regime and (ii) flattened-top shape caused by the generation of additional quantized vorticity by the high-amplitude second-sound wave.

was derived for moderate values of L not requiring screening corrections (for details, see Refs. [8,21]); the calculated L values may therefore differ from reality by up to $\approx 30\%$.

III. EXPERIMENTAL RESULTS

Figure 2 shows the voltage amplitude across the calibrated temperature sensor [18–20] during frequency sweeps across the resonances for the first two longitudinal resonances measured at 1.65 K for various heater powers. In agreement with previous results of Kotsubo and Swift [10,11] and Chagovets [12], we observe a crossover between two distinctly different shapes of the longitudinal second-sound resonances. At low drives, the Lorentzian shape of the resonances with the amplitude directly proportional to the driving power indicates a linear damping regime. Upon increasing the drive, the shape changes, resulting in flat-top peaks above some critical amplitude, as a new, nonlinear dissipation mechanism sets in. In accord with Refs. [10,11], as the power is increased further, the flattened peaks become broader and overall dissipation increases as well, while the level of the flattened top remains approximately constant. This is a signature of turbulent flow in the resonator, as quantized vortices are generated above the critical amplitude, over an increasingly wider frequency range around the resonance. This behavior appears qualitatively similar when measured at 1.45 K and 1.83 K.

Our experimental setup allows us to present direct proof of quantum vortex generation in oscillatory counterflow by simultaneously tracking the in-phase amplitude of a weakly driven transversal resonant second-sound wave. This is shown in Fig. 3 for a few selected heater powers driving the first longitudinal harmonic mode, in both linear and nonlinear damping regimes at 1.45 K. The true tracking of the transversal second-sound resonance is secured via a procedure described in detail in Refs. [21,23]. The attenuation of the transversal wave due to additional quantized vorticity in

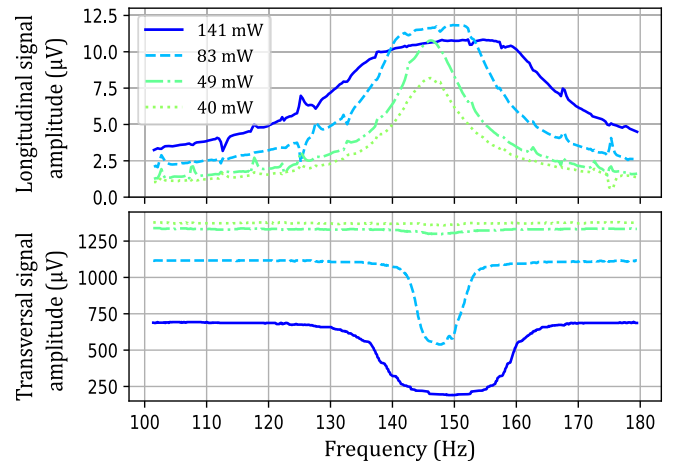


FIG. 3. Top: Selected frequency sweeps of the first harmonic mode at 1.45 K. Bottom: The simultaneously measured resonant amplitude of transversal second-sound wave propagating perpendicularly across the center of the resonator. The attenuation of the transversal signal clearly corresponds to the saturation part of the longitudinal amplitude, proving the generation of quantized vorticity in the superfluid component. In both panels, the horizontal axis represents the frequency of the voltage supplied to the heater.

the resonator clearly corresponds to the amplitude saturation of the longitudinal signal.

Figure 4 compares the evolution of the peak amplitude of the longitudinal signal with the vortex line density L in the center of the resonator calculated using Eq. (4) at 1.45 K as a function of the applied heater power. The top panel shows

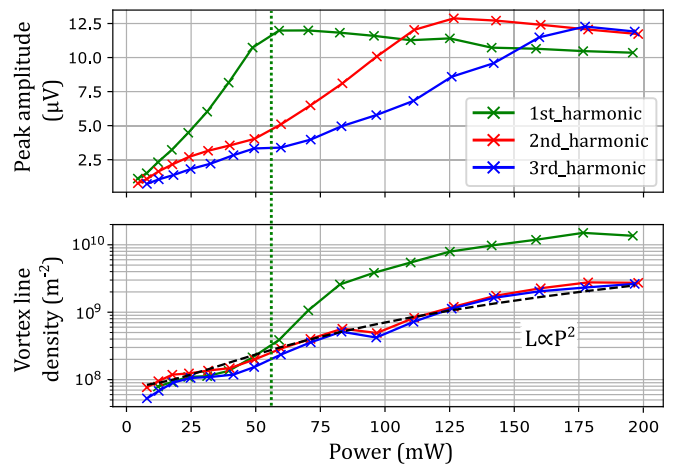


FIG. 4. Top: Power evolution of the peak amplitude of longitudinal second sound for first three modes at 1.45 K. Amplitude saturation implies the generation of quantized vorticity by the ac counterflow. Bottom: The corresponding vortex line density, L , measured in the center of the channel. The black dashed line represents the power law $L \propto P^2$, for vorticity originating from the dc counterflow alone. The green vertical dotted line indicates the critical power for the first mode, where both signals show generation of quantized vortices in the antinode of the longitudinal resonance. The lack of observation of any additional vortex line density for the second mode confirms the antinodal localization of vortex generation.

TABLE I. Critical values of heat flux for turbulent transition in oscillatory counterflow for different harmonic modes, estimated at three temperatures.

Harmonic mode	T K	\dot{q}_{crit} mW/cm ²
First	1.45	55
	1.65	85
	1.83	115
Second	1.45	120
	1.65	195
	1.83	—
Third	1.45	175
	1.65	—
	1.83	—

similar behavior for all three harmonic modes: the peak amplitude rises approximately linearly with the heating power and then saturates. The critical power values, for which the amplitude saturation occurs, have been found for all presented harmonic modes at 1.45 K. For experimental reasons, it was not possible to reach saturation with all modes at higher temperatures 1.65 K and 1.83 K. The observation is also partially masked by a rather strong background vortex line density due to the dc counterflow carrying the applied power in the resonator to the surrounding helium bath. The frequency dependence of the critical power is clearly seen; we shall discuss it in the next section.

All estimated values of critical heater power determined from the onset of saturation of amplitude of the longitudinal signal are shown in Table I. Note that critical conditions for turbulent transition were not reached for all cases, as the same heating power generates lower counterflow velocity at temperatures of 1.65 K and 1.83 K than at 1.45 K, in accord with Eq. (2).

IV. DISCUSSION

First, let us discuss possible caveats and experimental difficulties. The analysis of our data described above must be treated as semiquantitative for the following reason. While generating the steady-state quantum turbulence, we continuously apply heat typically of order 0.1 W to the He II sample inside the resonator, which must be carried to the surrounding helium bath. Our resonator is made of brass with walls about 1 cm thick. Assuming that the applied heat is conducted via brass walls, a simple estimate would lead to a temperature difference of order 1 K between the He II sample in the resonator and the helium bath, about three orders of magnitude higher than what is experimentally observed. For evidence, see, e.g., Fig. 2 which shows only a slight shift of the resonance frequency of the measured second-sound harmonics with the applied heat flux—the position of resonance would have followed the changes of the second-sound velocity with the increasing temperature of He II inside the resonator. We are therefore led to conclude that the applied heat is carried away from the He II sample in the resonator by a much more efficient mechanism—thermal counterflow, specifically by the normal component carrying the entropy through gaps between

the brass plugs, second-sound sensors, and the brass body of the resonator.

It is difficult to characterize the geometry of such counterflow in our experiment as well as in the experiments cited above and to judge how much these thermally driven flows affect our considerations below. We attempted to compensate the steady heat flux supplied by the heater, Eq. (1), by the same steady heat flux from an additional heater placed at the opposite end of the resonator. This, however, resulted in an increase of attenuation of the transverse second sound, indicating an increase of effective vortex line density in the center of the resonator. This suggests that a significant part of the heat exits the resonator via gaps adjacent to the second-sound sensors rather than via gaps between the brass plugs and the body of the resonator at its ends. We therefore treat the vortex line density in the center of the resonator generated at frequencies of longitudinal second-sound resonances simply as a heat flux-dependent background. Bearing in mind this caveat, we now attempt to determine the peak counterflow velocity of the studied oscillatory counterflow that corresponds to the applied ac heat flux.

A. Determination of critical velocity

Two different approaches may be employed. The first one is based on the idea that the peak counterflow velocity $v_{ns,ac}^I$ (i.e., its antinodal amplitude) is the same as that in the dc case [given by Eq. (2)] but resonantly enhanced by the quality factor Q , found to be of order 10:

$$v_{ns,ac}^I = Q \frac{\dot{q}_{ac}}{ST\rho_s}. \quad (5)$$

We stress that this approach is valid only in the linear damping regime, when the observed resonances are of Lorentzian shape. In the turbulent regime, further increase of the peak counterflow velocity is suppressed by the action of the mutual friction force.

The second and perhaps more straightforward way to determine the peak velocity is based on the direct measurement of the magnitude of the temperature variations δT in the resonator. The same approach was used by Kotsubo and Swift [10,11], who assumed a harmonic time dependence and spatial profile of the resonant standing wave. Following the same reasoning that leads to Eq. (13) in Ref. [11], we find the peak oscillatory counterflow velocity as

$$v_{ns,ac}^{II} = \frac{\rho_S}{u_2\rho_n}\delta T, \quad (6)$$

where u_2 stands for the second-sound velocity. The amplitude of the temperature oscillations δT can be determined from the ac voltage measured across the calibrated resistive thermometer biased by a constant current. The velocity determined in this manner should hold over the entire range of applied heat fluxes, as it is calculated from experimentally observed quantities.

On the other hand, discrepancies between the determined values of $v_{ns,ac}^I$ and $v_{ns,ac}^{II}$ in the subcritical region and observation of an additional phase shift, which both occurred for higher harmonics, suggest that either the thermal inertia together with the Kapitza resistance at the heater or the

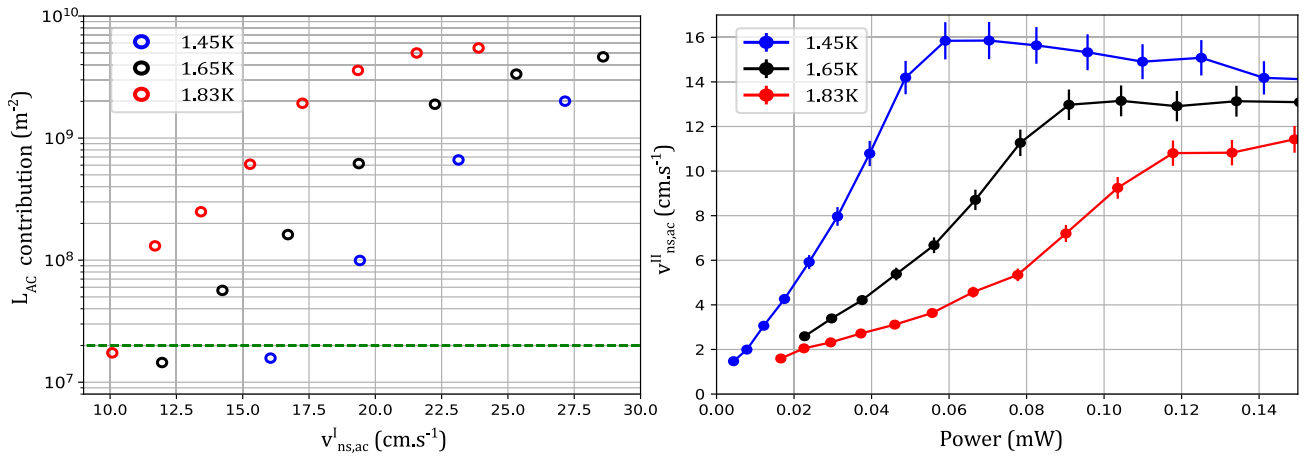


FIG. 5. Left: Contribution to vortex line density due to oscillatory counterflow (difference of values observed for first and second modes), plotted as a function of the velocity $v_{ns,ac}^I$. The rapid increase of vortex line density above the noise level (highlighted by the green dashed line) indicates the position of the critical velocity. Right: Oscillatory counterflow velocity $v_{ns,ac}^{II}$ obtained from the amplitudes of longitudinal resonances via Eq. (6) plotted as a function of heating power. The onset of saturation of $v_{ns,ac}^{II}$ determines the critical velocity. The error bars represent the fluctuations of the bias current supplied to the thermometer.

thermalization time constant of the used thermometer may affect the measurements at frequencies higher than the first fundamental mode, and thus may influence the temperature wave amplitude reading as well as the actual, slightly smoothed, heat flux amplitude delivered to the liquid which may be lower than Eq. (1) suggests. Indeed, the values of the critical heat flux amplitude measured at $T = 1.45$ K for first three harmonics, given in Table I, grow somewhat faster than with the square root of frequency, predicted for both classical [24] and quantum [25–27] oscillatory flows. For these reasons, we have limited deduction of critical oscillatory counterflow velocities for further quantitative analysis to the data measured using the first harmonic mode, where good agreement is obtained in the linear damping regime for both methods of determination of the peak counterflow velocity.

Let us now discuss the critical velocities determined by these two different approaches. In the left panel of Fig. 5, we plot the difference of vortex line density measured for the first harmonic mode (containing both ac and dc contributions) and second harmonic mode (giving the dc contribution only) as a function of $v_{ns,ac}^I$. The critical velocity can be determined from the onset of vortex line density (above the noise level, taken as 10% of the background due to dc counterflow near the critical power) and must be directly connected to a transition in the oscillatory counterflow accompanied by a rapid increase of quantized vortex generation. The second approach, via directly measured temperature oscillations in the channel, leads to the values of $v_{ns,ac}^{II}$, see the right panel of Fig. 5 showing the counterflow velocity obtained from the amplitudes of longitudinal resonances as a function of heater power. The saturation of this velocity marks the same transition as above and, moreover, indicates the longitudinal resonance as the energy supply for the additional vorticity, see also Refs. [10–12]. The critical velocities are listed below in Table II, showing quantitative agreement of the two approaches. In both cases, we estimate the uncertainty to be of order 1 cm/s, caused by the subjectivity of noise level determination and/or thermometer bias current fluctuations.

B. Comparison with other experiments

With these data at hand, we may turn to the broader discussion of the transition to quantum turbulence in various oscillatory He II flows generated mechanically, thermally, and by second sound in the frame of the two-fluid model.

Historically, the two-fluid model description of independent and coupled oscillatory flows of the normal and superfluid components was already considered by Donnelly and Penrose [15] in 1956 in an attempt to explain the experimentally observed crossover between two regimes of U-tube oscillations. Although the notion of quantized vortices and their role for the mutual friction force was not yet widely appreciated, their approach was capable of formally explaining the existence of the two observed decay regimes, assuming that at low velocity the two fluids move independently and their motion becomes gradually coupled upon reaching some critical velocity and eventually they move as a single fluid, i.e., in coflow. The length scale relevant to the (uncoupled) normal flow is the viscous penetration depth $\delta_n = \sqrt{2\eta/\rho_n\omega} \approx 70 - 200 \mu\text{m}$, where η is the dynamic viscosity. This scale is significantly smaller than the diameter of the U tubes (≈ 1 cm); we therefore deal with flows of high Stokes number, defined as $\text{St} = D^2/(\pi\delta_n^2)$, similarly to the counterflow experiments presented here.

TABLE II. Critical oscillatory counterflow velocities and corresponding critical Donnelly numbers obtained by two different approaches for all studied temperatures. See the text for details.

T K	Critical $v_{ns,ac}^I$ cm/s	Dn_{cr}^I	Critical $v_{ns,ac}^{II}$ cm/s	Dn_{cr}^{II}
1.45	17	15.6	16	14.7
1.65	12.5	15.3	13	15.9
1.83	10	13.2	11	14.5

1. Normal fluid critical velocity

Dynamical similarity and instabilities in high-Stokes-number oscillatory flows of He II have recently been studied by Schmoranzner *et al.* [16]. It was shown, based on systematic measurements of oscillatory He II flows due to various oscillators, that an instability leading to the turbulent transition can occur either in the normal or in the superfluid component of He II. For low velocities, only viscous drag is offered by the normal fluid, obeying a universal scaling law in terms of the suitably defined drag coefficient and the Donnelly number (boundary-layer-based Reynolds number), defined as

$$\text{Dn} = \delta_n v_n / \nu_n, \quad (7)$$

where v_n is the amplitude of normal fluid velocity. Upon exceeding a certain critical value of the Donnelly number, Dn_{cr} , the normal component undergoes a classical-like transition, also subsequently triggering the generation of quantized vortices in the superfluid component. The corresponding critical velocity of the normal component is denoted as $v_{n,\text{cr}}$.

2. Superfluid critical velocity

Even without the classical-like instability occurring as discussed above, quantized vorticity in the superfluid component may become generated via the Donnelly-Glaberson instability [28–30] at a dimensionless critical velocity $\hat{v}_{s,\text{cr}} = v_{s,\text{cr}} / \sqrt{\kappa\omega}$, where $v_{s,\text{cr}}$ is the dimensional superfluid critical velocity. Indeed, Hänninen and Schoepe [26,27] have argued that the onset of quantum turbulence in oscillatory flows of superfluid helium is universal, and can be derived from a general argument based on the “superfluid Reynolds number”. The critical velocity scales as $v_{s,\text{cr}} \propto \sqrt{\kappa\omega}$ with only the numerical prefactor depending somewhat on the geometry of the oscillating object because the flow velocity near the surface of the object may differ from the velocity amplitude of the body. A more detailed analysis derived from the dynamics of the turbulent state gives the criterion [27]

$$v_{s,\text{cr}} \approx \sqrt{8\kappa\omega/\beta}, \quad (8)$$

where the numerical factor β is about unity and depends on the mutual friction parameters.

Hänninen and Schoepe [26] evaluated β for several temperatures: $\beta = 1$ below 1 K, $\beta = 0.95$ (at 1.3 K), 0.89 (at 1.6 K), and 0.79 (at 1.9 K); which implies a slow *increase* of v_c by about 10% and gives fair agreement with experimental results obtained over a wide temperature range from below 0.4 K up to 1.9 K with a sphere 100 μm in diameter oscillating at 236 Hz, as displayed in Fig. 3 of Ref. [26].

It must be noted that virtually the same approach was used to analyze the turbulent instability in oscillatory counterflow in Refs. [10–12] without any consideration of a possible classical-like instability in the normal component. This resulted in the observation of a strong and systematic temperature dependence of superfluid critical velocities that the employed dynamical scaling theory could not explain [10,11], as the temperature dependence of β in Eq. (8) is too weak to account for critical velocities differing by a factor of 4 (see, e.g., Fig. 4 in Ref. [10]).

3. Interplay of the two instabilities

Which instability, i.e., either classical hydrodynamic instability of laminar flow of the normal component upon reaching a critical velocity $v_{n,\text{cr}}$ or Donnelly-Glaberson instability in the superfluid component upon reaching $v_{s,\text{cr}}$ occurs first depends both on the geometry of the oscillator and on the temperature, which determines the dynamic viscosity of He II and the densities of the two components. A crossover between the two outlined mechanisms of turbulence generation is possible and has indeed been observed in flows due to mechanical oscillators [16].

A similar approach may be applied to oscillatory counterflow, with one distinction. In experiments on flow due to mechanical resonators, the comparison of the two criteria for the transition is straightforward, as in coflow, the velocities of the normal and superfluid components are practically identical. However, in counterflow $v_n \neq v_s$, hence a common dimensionless parameter must be found for both types of instability to facilitate such a comparison. For this purpose, the superfluid critical velocity $v_{s,\text{cr}}$ may be converted to an effective critical Donnelly number $\text{Dn}_{\text{cr,eff}}$ using

$$\text{Dn}_{\text{cr,eff}} = \frac{\delta_n v_{s,\text{cr}} \rho_s}{\rho_n \nu_n}. \quad (9)$$

This is the same formal definition of Dn_{cr} as given below Eq. (7), with the critical normal fluid velocity formally expressed as $v_{n,\text{cr}} = \rho_s / \rho_n v_{s,\text{cr}}$, i.e., as the peak normal fluid velocity in the oscillating thermal counterflow at the very first occurrence of the Donnelly-Glaberson instability in the superfluid component oscillating with the critical velocity $v_{s,\text{cr}}$.

Unlike the true critical Donnelly number describing the classical instability Dn_{cr} , the critical value of $\text{Dn}_{\text{cr,eff}}$ is no longer expected to be constant. On the contrary, requiring a constant value of the correct critical parameter, $\hat{v}_{s,\text{cr}}$, also requires $\text{Dn}_{\text{cr,eff}}$ to be a function of temperature. However, $\text{Dn}_{\text{cr,eff}}$ will be independent of the frequency of oscillations, as both $v_{n,\text{cr}}$ and $v_{s,\text{cr}}$ have the same frequency dependence, with either critical velocity $\propto \sqrt{f}$.

We stress that, assuming no or perhaps a very low number of remnant quantized vortices at low flow velocities, this classical-like instability is not affected by the potential flow of the superfluid component; as mutual friction is nearly absent. This allows us to apply the described model to oscillatory coflows as well as counterflows and in particular to the experiments discussed here.

First, using our data, we have described two different approaches to determine critical counterflow velocities $v_{ns,\text{ac}}^{\text{I}}$ and $v_{ns,\text{ac}}^{\text{II}}$. Requiring zero net mass flow, we can calculate the corresponding peak critical velocities of the oscillating normal fluid. Application of a no-slip boundary condition then leads to critical Donnelly numbers $\text{Dn}_{\text{cr}}^{\text{I}}$ and $\text{Dn}_{\text{cr}}^{\text{II}}$, also given in Table II. We note that for this calculation we naturally use the frequency of the longitudinal second sound, i.e., twice the frequency of the applied oscillatory heat flux. Over the temperature range 1.45–1.83 K (where the normal fluid density changes about five times) the critical Donnelly numbers are approximately constant $\text{Dn}_{\text{cr}}^{\text{I}} \cong \text{Dn}_{\text{cr}}^{\text{II}} \cong 15 \pm 2$, providing a good quantitative characterization of the turbulent instability.

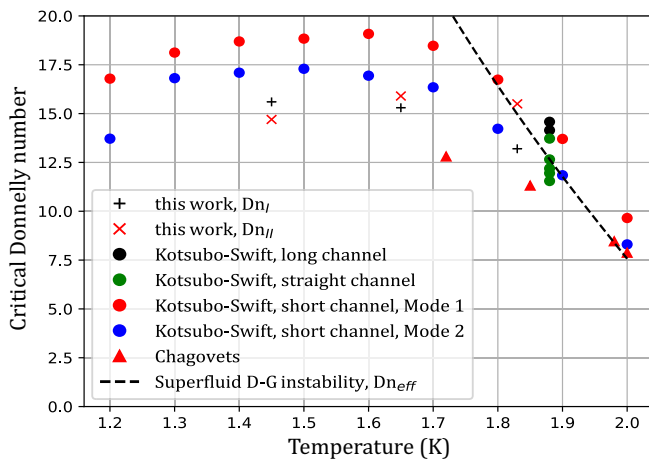


FIG. 6. Temperature dependence of the critical Donnelly number for oscillatory thermal counterflow as determined from this work and the experiments of Kotsubo and Swift [10,11] and Chagovets [12]. The dashed line represents an effective Donnelly number calculated for the instability based on the Hänninen-Schoepe criterion, Eqs. (8) and (9).

Second, we calculate critical Donnelly numbers based on the data measured for mechanically generated ac counterflow of He II at 1.88 K by Kotsubo and Swift, Dn_{cr}^{KS} , based on Fig. 5 of Ref. [11], showing critical counterflow velocities from the first two modes in their long resonator and the first five modes in their straight resonator, covering more than a decade of second-sound frequencies. All values of critical Donnelly numbers obtained at this temperature fall within a narrow interval $Dn_{cr}^{KS} = 13 \pm 2$, in fair agreement with our measurements. Furthermore, we have used Fig. 6 of Ref. [11], displaying the scaled temperature dependence of the critical velocities from the first two modes measured in their short resonator. The calculated critical Donnelly numbers are shown in Fig. 6, appearing approximately constant between 1.2 K and 1.7 K, $Dn_{cr}^{KS} \cong 17 \pm 2$, with a pronounced decreasing tendency at higher temperatures.

Finally, we may compare with the critical Donnelly numbers Dn_{cr}^{Ch} for thermally generated ac counterflow of He II estimated using the data measured by Chagovets in an epoxy cylindrical resonator of diameter 7 mm, 3.5 cm long, at four temperatures between 1.72 K and 2.0 K, specifically the data series shown in Fig. 2 of Ref. [12]. For example, at $T = 1.85$ K we estimate the saturated amplitude of the temperature oscillations $\delta T \approx 0.8$ mK that starts to flatten upon reaching about 32 mW/cm² of applied heat flux, and the fundamental resonant frequency of second sound $f = 197$ Hz. Similarly, we read the available data for 1.72, 1.98, and 2.0 K and, using the known temperature dependence of the second-sound velocity, we calculate the relevant frequencies of the fundamental mode at these temperatures. These data, together with tabulated values of He II properties [22] allow us to calculate, using Eq. (6), the velocity $v_{ns,ac}^{II}$ and, subsequently, the critical Donnelly number Dn_{cr}^{Ch} , also shown in Fig. 6.

It is remarkable that, within the experimental accuracy, in the temperature range from 1.2 K to 1.7 K, three different

experiments: (i) mechanically driven second sound [10,11], (ii) thermally driven counterflow by Chagovets [12], as well as (iii) our own display the onset of the transition to quantum turbulence characterized by the same critical Donnelly number $Dn_{cr} \approx 16 \pm 3$. This strongly suggests that the transition is triggered when the instability in oscillatory laminar flow of the viscous normal component of He II is reached. In the given temperature range, the transition thus cannot be described by the dynamical scaling theory used in Refs. [10,11], which deals solely with superfluid instabilities.

However, the data of Refs. [11,12] show a departure from this value of Dn_{cr} as the temperature is increased above ≈ 1.8 K, which is fully explained by the instability in the superfluid component—production of quantized vorticity by means of the Donnelly-Glaberson mechanism. The data are summarized in Fig. 6, where the effective Donnelly number, Dn_{eff} , for this instability is shown, as calculated based on Eqs. (9) and (8). Hence, we clearly observe a crossover of two different mechanisms of turbulence generation in oscillatory counterflow: one related to a classical instability of the normal fluid dominating at lower temperatures in the two-fluid regime, while the other is purely a consequence of quantized vortex dynamics in the superfluid component and dominates at higher temperatures.

It is interesting to note that oscillating coflow, e.g., due to a quartz tuning fork [16], is similar in that it displays the same general crossover between these two mechanisms. However, the respective temperature intervals are inverted—the classical instability dominates closer to the lambda point and the superfluid one at lower temperatures. It is naturally understood that the behavior of oscillating thermal counterflow is different in this sense, as the equation of continuity requires that $v_s/v_n = \rho_n/\rho_s$, making it likely that the superfluid critical velocity is reached first when the ratio ρ_n/ρ_s is large.

C. Applicability of the obtained results

We have to emphasize that the above hydrodynamic approach is applicable only in the temperature range where superfluid ⁴He displays the two-fluid behavior. On lowering the temperature below 1 K, the mean-free path of phonons grows and soon becomes greater than the size of the system and, in the $T \rightarrow 0$ limit, only the superfluid component exists, hence the very concept of thermal counterflow becomes poorly defined. Still, transition to quantum turbulence occurs in a variety of oscillatory flows, displaying interesting features such as multiple critical velocities [31,32] and hysteretic [33–35] or switching phenomena [36,37]; for reviews, see Refs. [13,14] and references therein. These features fall outside the scope of this paper.

V. CONCLUSIONS

We have presented experimental work on thermally generated oscillatory counterflow in a closed square-cylinder-shaped second-sound resonator, and directly proven generation of quantized vortices in the antinode of the fundamental longitudinal standing wave using the second-sound attenuation technique.

Comparison with studies of oscillatory flows due to mechanical resonators in ^4He [16] and previous thermally and mechanically driven second-sound experiments [10–12] reveal that the instabilities marking the turbulent transition in all these flows are of the same type. Namely, (i) a classical-like instability in the flow of the viscous normal component occurring upon reaching the critical Donnelly number Dn_{cr} and (ii) the Donnelly-Glaberson instability in the superfluid component leading to vortex multiplication due to self-reconnections.

A crossover between these two mechanisms is observed, while the temperature is varied across the interval corresponding to the two-fluid regime. This strongly suggests, perhaps surprisingly, that transition to turbulence in oscillatory coflow and counterflow is governed by the same underlying physics, although the crossover occurs in the opposite direction for counterflow than for coflow.

We have also shown that the Hänninen and Schoepe criterion for critical superfluid velocity [26,27] (relationship 8) and similar approaches based on quantized vortex dynamics

cannot be considered universal in the two-fluid regime, as instabilities of the normal fluid flow are not taken into account. On the other hand, these same criteria remain useful for the description of the superfluid instability and recover universality at very low temperatures, where the two-fluid model is no longer applicable. However, in the two-fluid regime above ≈ 1 K, they must be complemented by a suitable description of the classical-like instabilities of the normal component.

It remains to be seen how the present analysis extends into dc counterflow experiments and how the two described instabilities relate to the T-I and T-II turbulent states observed by Tough [7], and we hope that our work stimulates further research into this area.

ACKNOWLEDGMENTS

The authors appreciate the help of E. Varga at the early stage of the experiments and acknowledge the support by the Czech Science Foundation under Project No. GAČR 20-00918S.

-
- [1] C. F. Barenghi, L. Skrbek, and K. R. Sreenivasan, Introduction to quantum turbulence, *Proc. Natl. Acad. Sci. U.S.A.* **111**, 4647 (2014).
- [2] W. F. Vinen and J. J. Niemela, Quantum turbulence, *J. Low Temp. Phys.* **128**, 167 (2002).
- [3] R. J. Donnelly, *Quantized Vortices in Helium II* (Cambridge University Press, Cambridge, 1991).
- [4] L. Skrbek, D. Schmoranzer, Š. Midlik, and K. R. Sreenivasan, Phenomenology of quantum turbulence in superfluid helium, *Proc. Natl. Acad. Sci. U.S.A.* **118**, e2018406118 (2021).
- [5] M. L. Baehr and J. T. Tough, Critical Velocity in Two-Fluid Flow of He II, *Phys. Rev. Lett.* **53**, 1669 (1984).
- [6] W. F. Vinen, Mutual friction in a heat current in liquid helium II, I. Experiments on steady heat currents, *Proc. R. Soc. London A* **240**, 114 (1957); II. Experiments on transient effects, **240**, 128 (1957); III. Theory of the mutual friction, **242**, 493 (1957); IV. Critical heat currents in wide channels, **243**, 400 (1958).
- [7] J. T. Tough, *Superfluid turbulence*, in *Progress in low temperature physics* (North-Holland Publishing Co., Amsterdam, 1982), Vol. VIII.
- [8] S. Babuin, M. Stammeier, E. Varga, M. Rotter, and L. Skrbek, Quantum turbulence of bellows-driven ^4He superflow: Steady state, *Phys. Rev. B* **86**, 134515 (2012).
- [9] S. Babuin, E. Varga, W. F. Vinen, and L. Skrbek, Quantum turbulence of bellows-driven ^4He superflow: Decay, *Phys. Rev. B* **92**, 184503 (2015).
- [10] V. Kotsubo and G. W. Swift, Vortex Turbulence Generated by Second Sound in Superfluid ^4He , *Phys. Rev. Lett.* **62**, 2604 (1989).
- [11] V. Kotsubo and G. W. Swift, Generation of superfluid vortex turbulence by high-amplitude second sound in ^4He , *J. Low Temp. Phys.* **78**, 351 (1990).
- [12] T. V. Chagovets, Electric response in superfluid helium, *Physica B* **488**, 62 (2016).
- [13] L. Skrbek and W. F. Vinen, The use of vibrating structures in the study of quantum turbulence, in *Progress in Low Temperature Physics*, edited by M. Tsubota and W. P. Halperin (Elsevier, Amsterdam, 2009), Vol. XVI, Chap. 4.
- [14] W. F. Vinen and L. Skrbek, Quantum turbulence generated by oscillating structures, *Proc. Natl. Acad. Sci. U.S.A.* **111**, 4699 (2014).
- [15] R. J. Donnelly and O. Penrose, Oscillations of liquid helium in a U-tube, *Phys. Rev.* **103**, 1137 (1955).
- [16] D. Schmoranzer, M. J. Jackson, Š. Midlik, M. Skyba, J. Bahyl, T. Skoknkov, V. Tsepelin, and L. Skrbek, Dynamical similarity and instabilities in high-Stokes-number oscillatory flows of superfluid helium, *Phys. Rev. B* **99**, 054511 (2019).
- [17] D. D. Awschalom and K. W. Schwarz, Observation of a Remanent Vortex-Line Density in Superfluid Helium, *Phys. Rev. Lett.* **52**, 49 (1984).
- [18] microsensor.com.ua
- [19] V. F. Mitin, P. C. McDonald *et al.*, Ge-on-GaAs film resistance thermometers for cryogenic applications, *Cryogenics* **47**, 474 (2007).
- [20] V. F. Mitin, V. V. Kholevchuk, and B. P. Kolodych, Ge-on-GaAs film resistance thermometers: Low-temperature conduction and magnetoresistance, *Cryogenics* **51**, 68 (2011).
- [21] E. Varga, M. J. Jackson, D. Schmoranzer, and L. Skrbek, The use of second sound in investigations of quantum turbulence in He II, *J. Low Temp. Phys.* **197**, 130 (2019).
- [22] R. J. Donnelly and C. F. Barenghi, The observed properties of liquid helium at the saturated vapor pressure, *J. Phys. Chem. Ref. Data* **27**, 1217 (1998).
- [23] E. Varga, S. Babuin, V. S. Lvov, A. Pomyalov, and L. Skrbek, Transition to quantum turbulence and streamwise inhomogeneity of vortex tangle in thermal counterflow, *J. Low Temp. Phys.* **187**, 531 (2017).
- [24] M. Blažková, D. Schmoranzer, and L. Skrbek, Transition from laminar to turbulent drag in flow due to a vibrating quartz fork, *Phys. Rev. E* **75**, 025302(R) (2007).
- [25] M. Blažková, D. Schmoranzer, L. Skrbek, and W. F. Vinen, Generation of turbulence by vibrating forks and

- other structures in superfluid ^4He , *Phys. Rev. B* **79**, 054522 (2009).
- [26] R. Hänninen and W. Schoepe, Universal critical velocity for the onset of turbulence of oscillatory superfluid flow, *J. Low Temp. Phys.* **153**, 189 (2008).
- [27] R. Hänninen and W. Schoepe, Universal onset of quantum turbulence in oscillating flows and crossover to steady flows, *J. Low Temp. Phys.* **158**, 410 (2010).
- [28] D. K. Cheng, M. W. Cromar, and R. J. Donnelly, Influence of an Axial Heat Current on Negative-Ion Trapping in Rotating Helium II, *Phys. Rev. Lett.* **31**, 433 (1973).
- [29] W. I. Glaberson, W. W. Johnson, and R. M. Ostermeier, Instability of a Vortex Array in He II, *Phys. Rev. Lett.* **33**, 1197 (1974).
- [30] R. M. Ostermeier and W. I. Glaberson, Instability of vortex lines in the presence of axial normal fluid flow, *J. Low Temp. Phys.* **21**, 191 (1975).
- [31] H. A. Nichol, L. Skrbek, P. C. Hendry, and P. V. E. McClintock, Flow of He II Due to an Oscillating Grid in the Low-Temperature Limit, *Phys. Rev. Lett.* **92**, 244501 (2004).
- [32] D. Schmoranzner, M. J. Jackson, V. Tsepelin, M. Poole, A. J. Woods, M. Človečko, and L. Skrbek, Multiple critical velocities in oscillatory flow of superfluid ^4He due to quartz tuning forks, *Phys. Rev. B* **74**, 214503 (2006).
- [33] J. Jger, B. Schuderer and W. Schoepe, Turbulent and Laminar Drag of Superfluid Helium on an Oscillating Microsphere, *Phys. Rev. Lett.* **74**, 566 (1995).
- [34] D. Charalambous, L. Skrbek, P. C. Hendry, P. V. E. McClintock and W. F. Vinen, Experimental investigation of the dynamics of a vibrating grid in superfluid ^4He over a range of temperatures and pressures, *Phys. Rev. E* **74**, 036307 (2006).
- [35] R. Goto, S. Fujiyama, H. Yano, Y. Nago, N. Hashimoto, K. Obara, O. Ishikawa, M. Tsubota, and T. Hata, Turbulence in Boundary Flow of Superfluid ^4He Triggered by Free Vortex Rings, *Phys. Rev. Lett.* **100**, 045301 (2008).
- [36] M. Niemetz and W. Schoepe, Stability of laminar and turbulent flow of superfluid He-4 at mK temperatures around an oscillating microsphere, *J. Low Temp. Phys.* **135**, 447 (2004).
- [37] N. Hashimoto, A. Handa, M. Nakagawa, K. Obara, H. Yano, O. Ishikawa, and T. Hata, Switching phenomena between laminar and turbulent flows of superfluid ^4He generated by a vibrating wire, *J. Low Temp. Phys.* **148**, 299 (2007).